Vanadia–silica mixed oxides. Influence of vanadia precursor, drying method and calcination temperature on structural and chemical properties

Dominique C. M. Dutoit, Michael Schneider, Patrizia Fabrizioli and Alfons Baiker*

Department of Chemical Engineering and Industrial Chemistry, Swiss Federal Institute of Technology, ETH-Zentrum, CH-8092 Zürich, Switzerland

The effects of vanadium precursor, drying procedure and calcination temperature, decisive for the chemical, structural and textural properties of sol–gel-derived vanadia–silica mixed oxides, have been studied. Vanadium(III) acetylacetonate and vanadium(V) oxide triisopropoxide were used as precursors with largely different reactivities. The vanadia–silica mixed oxides were prepared *via* the sol–gel method, involving acid catalysis together with pre-hydrolysis and gelation forced by the addition of ammonia. The as-prepared gels were dried evaporatively (xerogels), dried supercritically by semicontinuous extraction with supercritical CO_2 at 313 K (low-temperature aerogels) or high-temperature supercritically dried (high-temperature aerogels). The mixed oxides were characterized by N_2 physisorption, XRD, FTIR, FT-Raman, XPS and diffuse reflectance UV–VIS spectroscopy. Vanadia–silica aerogels derived from vanadium(III) acetylacetonate, which possesses much lower reactivity than vanadium(V) oxide triisopropoxide, had textural properties similar to those of silica and exhibited a low vanadia surface concentration. Higher vanadium surface concentrations were detected for samples derived from vanadium(V) oxide triisopropoxide, as indicated by XPS analysis. Supercritical drying led to mesoporous samples. Vanadia remained well dispersed in the gels dried at low temperature (low-temperature aerogel, xerogel) even after calcination in air at 873 K. In contrast, the high-temperature aerogels showed significant agglomeration and crystallisation upon calcination. The studies indicate that the choice of the vanadium precursor and drying procedure are crucial parameters for controlling segregation–agglomeration and/or crystallisation of well dispersed vanadia and thus tailoring the vanadium surface concentration.

Recently, we have shown that highly dispersed, mesoporous vanadia–silica mixed oxides with up to 20 mass% V_2O_5 content can be prepared *via* a sol–gel route including acid catalysis together with pre-hydrolysis and subsequent removal of the alcoholic solvent by semicontinuous extraction with supercritical CO_2.[1] Variation of the vanadia content distinctly influenced the textural properties, composition and structure of the vanadia phase, whereas ageing in a basic medium predominantly affected the BET surface area and porosity.

Acid catalysis together with pre-hydrolysis proved to be important for preparing highly dispersed vanadia–silica mixed oxides. Another influential factor is the dependence of sol–gel reactivity on the precursor used.[2–4] In general, hydrolysis and condensation are influenced strongly by the nature of both the organic ligand and the metal centre (*e.g.* V^{5+} *vs.* V^{3+}).[5–9] As regards the impact of drying, a comparison between evaporative drying, leading to xerogels, and supercritical drying *via* either semicontinuous extraction with supercritical CO_2 (low-temperature variant) or direct removal of the solvent above its critical temperature (high-temperature route), both resulting in aerogels, revealed prominent effects on the textural, structural and catalytic properties of titania–silica mixed oxides.[2,10] These effects originate mainly from the differences in the differential drying stresses[2,11–13] and operating temperature.[2,13]

In this work, we have extended our previous study on the structural and chemical tailoring of aerogels by considering the effects of a less reactive vanadia precursor and the application of different drying methods. $V^{III}(acac)_3$ is used instead of vanadium(V) oxide triisopropoxide (VOTIP) for synthesizing mesoporous, highly dispersed and thermally stable vanadia–silica mixed oxides. A comparison between xerogel, low-temperature aerogel and high-temperature aerogel reveals the prominent influence of the drying method on the structural and textural properties, thus offering another powerful tool for tailoring the resulting mixed oxides.

Experimental

Sample preparation

Throughout this work a set of acronyms is used, taking 10VHTac as an example. The first numeral displays the designed content of nominal V_2O_5 in mass%, based on the theoretical system V_2O_5–SiO_2 (10 mass% $\equiv$ V/(V + Si) = 6.8 %); V stands for vanadia–silica; the subsequent two capital letters represent the drying method used (LT, low-temperature supercritical drying; HT, high-temperature supercritical drying, X, xerogel); ac means vanadium(III) acetylacetonate was used as precursor instead of vanadium(V) oxide triisopropoxide.

Sol–gel preparation. The preparation procedure is described in detail in ref. 1. When vanadium(III) acetylacetonate [$V^{III}(acac)_3$; Fluka, pract.] was used as precursor instead of vanadium(V) oxide triisopropoxide (VOTIP; Gelest), the following procedure was applied. After cooling the pre-hydrolysed tetraethoxysilicon(IV) solution (TEOS; Fluka, *purum*) to ambient temperature, 5.83 g $V^{III}(acac)_3$, dissolved in a mixture of 40 ml ethanol (EtOH; Fluka, *puriss*, p.a.) and 12 ml acetylacetone (acac; Fluka, *puriss*, p.a.) by heating to 323 K for 10 min, was added. The sol was aged for 60 min at 323 K and for 14 h at ambient temperature. The gelation was forced by ammonium hydroxide (NH_4OH; Fluka, *puriss*, p.a.) diluted in EtOH ($V_{EtOH}:V_{NH_4OH} = 6:1$). First, 12 ml of the basic solution were added dropwise within 1 min. After 30 min another 6 ml was introduced and 5 min later a gel formed. For pure silica, the first addition of the basic solution sufficed to induce gelation.

Drying the sol–gel product. Three different drying methods were applied. (i) Evaporative drying (xerogels). The vanadia–silica gel was dried at 10 kPa and 313 K for 22 h and at 373 K for another 24 h, resulting in an olive material. (ii) High-temperature supercritical drying (high-temperature aerogels). The solution sol–gel (SSG) product was transferred in a

stainless-steel liner into an autoclave with a net volume of 1.09 dm^3. The corresponding critical data for EtOH, the dominating component of all SSG solvents used in this work, are: $V_c = 167$ ml mol^{-1}, $T_c = 516$ K, $p_c = 6.4$ MPa.[14] The high-pressure system was flushed with nitrogen, pressurized to 10 MPa, hermetically sealed and heated at 1 K min^{-1} to 533 K. The autoclave was kept at the final temperature for 30 min to ensure complete thermal equilibration. The final pressure was *ca.* 24 MPa. The pressure was then released isothermally at 0.1 MPa min^{-1}. Finally, the system was flushed with nitrogen and allowed to cool to ambient temperature. The resulting aerogel clumps were greyish-black. (iii) Semicontinuous extraction with supercritical carbon dioxide (low-temperature aerogels). This drying procedure has been described in detail in ref. 1. In brief, the solvent of the SSG product was extracted semicontinuously by a CO_2 flow of 20 g min^{-1} for 5 h (6 kg CO_2) at 24 MPa and 313 K. The carbon dioxide was then released isothermally at a rate of *ca.* 20 g min^{-1}, leading to colourless (10VLT) and beige (10VLTac) aerogel clumps.

Calcination procedure and composition analysis. Amounts of *ca.* 2 g of the as-prepared (raw) samples were ground in a mortar and then calcined in a tubular reactor with upward flow. To remove most of the organic residues, the aerogel samples were pretreated in a nitrogen flow of 0.5 dm^3 min^{-1} for 1 h prior to calcination. They were heated at 5 K min^{-1} to 673 K. After being cooled to *ca.* 353 K, they were heated again at 5 K min^{-1}, this time in air flowing at 0.5 dm^3 min^{-1}, and held for 5 h at 673 or 873 K. After calcination at 873 K all samples were bright yellow. The compositions of the samples were calculated based on the amounts used for preparation and confirmed independently by AAS analysis. The deviation of the two methods was $<10\%$. For the 10VLTac aerogel analysis revealed a V_2O_5 content of only 1.5 mass%. This indicates that the acetylacetonate precursor was probably not hydrolysed quantitatively during the sol–gel processing, resulting in an extraction of vanadium species during low-temperature supercritical drying. The total carbon content of the samples was determined with a LECO CHN-900 elemental microanalysis apparatus.

Physicochemical characterisation

The physicochemical properties of the aerogels were characterised by means of nitrogen physisorption, X-ray diffraction, vibrational spectroscopy, UV–VIS spectroscopy and XPS. Measurement conditions and procedures are described in detail in ref. 1.

Nitrogen physisorption. The specific surface areas (S_{BET}), mean cylindrical pore diameters ($\langle d_p \rangle$) and specific desorption pore volumes [$V_{p(N_2)}$] were determined by nitrogen physisorption at 77 K using a Micromeritics ASAP 2000 instrument. Prior to measurement, the raw samples were degassed for 16 h at 353 K and the calcined samples for 5 h at 473 K.

X-Ray diffraction. X-Ray analysis in the 2θ range 13–35° was carried out on a Siemens D5000 powder diffractometer in step mode using Cu-Kα radiation. A step size of 0.01° was used.

FTIR spectroscopy. IR spectra (transmission mode) of the samples calcined at 873 K were recorded on a Perkin-Elmer 2000 NIR–FT–Raman instrument. Mixtures of 0.7 mg catalyst sample and 100 mg dry KBr (Fluka) were ground finely and agglomerated under pressure (20 MPa, 220 s). The self-supporting sample wafers were mounted on a special sample holder in an environmental chamber. The sample cell was purged with a small flow of dried air during the measurements. Spectra were recorded at room temperature in the range 1400–700 cm^{-1} by accumulating 500 scans with a resolution of 4 cm^{-1}. The spectrum of dry KBr was taken for background subtraction.

For Ti^{4+} dispersed in silica[2,15,16] and for titanium silicalite[17] a vibrational band at *ca.* 960 cm^{-1} has been assigned to an asymmetric Ti—O—Si stretching mode. This band proved to be a pertinent tool for the semiquantitative estimate of the Si—O—Ti connectivity.[2] By analogy with titania–silica, the FTIR spectra of vanadia–silica mixed oxides are characterised by a band which can be attributed to an asymmetric stretching mode of SiO_4 tetrahedra connected to V ions. This band was found at *ca.* 960 cm^{-1} for vanadium silicalites[18–21] and at about 950 cm^{-1} for vanadia–silica xerogels.[22] Recently it has been shown that for oxovanadium centres dispersed in a silica matrix (vanadia–silica xerogel) a band in this range, previously assigned to the terminal V=O stretch,[23] is due to a basal plane V—O stretch.[15] With a unitary silica aerogel[1] as well as with silicalites,[17,24] a peak at 960 cm^{-1} associated with an Si—OH stretching mode was observed, indicating that silanol vibrations superimpose on the Si—O—V stretching mode.

For the evaluation of the FTIR results, four bands were deconvoluted into Gaussian curves, following the procedure described in ref. 1. The positions and corresponding assignments of these vibrations are as follows: (i) 800,[7,25] 810 cm^{-1} [26] for the symmetric ν(Si—O—V) stretching vibration; (ii) 950–960 cm^{-1} assumed for ν(Si—O—Si) vibrations[18–22] and 960 cm^{-1} for Si—OH vibrations;[1,17,24] (iii) 1080,[7] 1095,[26] 1080–1105 cm^{-1} [25] for the asymmetric ν(Si—O—Si) stretching vibration; (iv) 1180,[26] 1200,[25] 1220 cm^{-1} [7] for asymmetric ν(Si—O—Si) stretching vibrations.

For the deconvolution the starting values were chosen at 800, 950, 1080 and 1220 cm^{-1}. The deconvoluted band positions of the calcined vanadia–silica aerogels were in the ranges 779–810, 928–937, 1071–1085 and 1206–1220 cm^{-1}. In order to prevent any deterioration of the Si—O—V analysis, the contribution of the deconvoluted Si—OH peak area of a correspondingly pretreated silica aerogel was deducted from the peak areas of the binary aerogels, taking into account the SiO_2 content in atom%. The ratio $R = S_{Si—O—V}/S_{Si—O—Si}$ of the deconvoluted peak areas of the ν(Si—O—V) band at 928–937 cm^{-1} and of the ν(Si—O—Si) band at 1206–1220 cm^{-1} was used as an estimate of the relative proportions of Si—O—V entities in the mixed oxides, and thus reflects the mixing efficiency.

FT-Raman spectroscopy. For the Raman measurements the samples calcined at 873 K were introduced into a metallic sample holder with a 4 mm diameter cavity. Prior to measurement, the samples were dehydrated *in situ* by heating at a laser power of 0.9 W for 30 min, resulting in *ca.* 550 K. Spectra were excited using the 1064 nm line of an Nd:YAG laser and recorded with a Perkin-Elmer 2000 NIR–FT–Raman instrument. Spectra in the 1300–200 cm^{-1} wavenumber range were obtained by accumulating 512 scans at a spectral resolution of 8 cm^{-1} and using a laser power of 900 mW.

UV–VIS diffuse reflectance spectroscopy. UV–VIS spectra of the samples calcined at 873 K were measured on a Perkin-Elmer Lambda 16 spectrometer equipped with a 76 mm integration sphere. The diffuse reflectance spectra were recorded at room temperature using $BaSO_4$ as a reference. Prior to measurement, the samples were pretreated for 1 h at 410 K and 125 mbar and subsequently sealed. For presentation the spectra were converted to the Kubelka–Munk function.

XPS analysis. XPS analysis of the catalyst samples was carried out in a Leybold–Heraeus LHS 11 MCD instrument using Mg-Kα radiation (240 W) to excite photoelectrons. The base pressure of the chamber was 4×10^{-10} mbar, and the pressure during the measurements was 2×10^{-9} mbar. The analyser was operated at 150 eV constant pass energy at an

energy scale calibrated *vs.* the Au $4f_{7/2}$ signal at 84.0 eV. To compensate for the steady-state charging effects, binding energies were normalized with respect to the position of the C 1s signal, resulting from adsorbed hydrocarbon fragments.

Results

Textural properties and carbon contents of the aero(xero)gels, whether raw or calcined in air at different temperatures, are listed in Table 1.

Nitrogen physisorption

In general, the aerogels showed a type IV isotherm with a type H2 desorption hysteresis according to IUPAC classification,[27] which is characteristic of mesoporous materials. The uncalcined sample 10VHT exhibited a type H3 desorption hysteresis, which is usually observed with aggregates of plate-like particles giving rise to slit-shaped pores.[27] The BET surface areas, pore volumes and graphically assessed pore size maxima of the pore size distributions, derived from the desorption branches of all aerogel samples, raw and calcined in air at 673 and 873 K, were in the ranges 649–1103 $m^2\ g^{-1}$, 1.6–3.4 $cm^3\ g^{-1}$ and 14–25 nm, respectively (Table 1).

The use of $V^{III}(acac)_3$ instead of vanadium(v) oxide triisopropoxide as the vanadium precursor led to different textural properties. All samples, uncalcined and calcined in air at 673 or 873 K, derived from $V^{III}(acac)_3$ showed higher BET surface areas, pore volumes and graphically assessed pore size maxima than the corresponding samples prepared from vanadium(v) oxide triisopropoxide. Owing to the low vanadium content of the sample, the calcined aerogel series 10VLTac exhibited substantially higher micropore surface areas (S_t) and micropore volumes (V_t) compared to the corresponding samples of the 10VLT series, whereas the microporosity was in the same range for the high-temperature, supercritically dried samples 10VHT and 10VHTac. Moreover, the BET surface area and pore volume of 10VHTac were more resistant towards calcination in air at 873 K than those of 10VHT.

The pore size distributions and the *t*-plots of differently dried vanadia–silica materials are represented in Fig. 1. In contrast to both the high-temperature aerogel series 10VHT and the low-temperature series 10VLT, which showed type IV isotherms with type H2 desorption hysteresis, xerogel 10VX calcined at 673 or 873 K possessed a type I isotherm without desorption hysteresis,[27] which indicated a substantial amount of microporosity (Table 1). The graphically assessed pore size

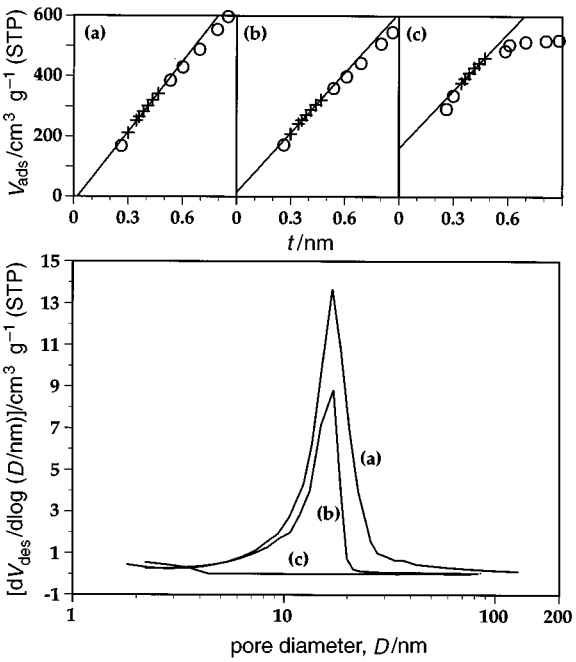

Fig. 1 Textural properties of differently dried vanadia–silica mixed oxides with 10 mass% nominal V_2O_5, calcined in air at 673 K. (a) High-temperature aerogel 10VHT; (b) low-temperature aerogel 10VLT; (c) xerogel 10VX. Bottom: differential pore-size distributions derived from the desorption branches of the physisorption isotherms; top: t-plot analysis (+points taken for linear regression). Sample designations are explained in the Experimental section.

maxima were in the range 14–25 nm for all aerogels and <2 nm for the xerogels. A comparison (Table 1) between the differently dried samples, calcined in air at 673 K, showed that mesoporosity decreased and microporosity increased in the order: high-temperature aerogel 10VHT [$V_{p(N_2)} = 3.2\ cm^3\ g^{-1}$, $S_t = 0\ m^2\ g^{-1}$], low-temperature aerogel 10VLT (1.8 $cm^3\ g^{-1}$, 53 $m^2\ g^{-1}$) and xerogel 10VX (0.2 $cm^3\ g^{-1}$, 245 $m^2\ g^{-1}$). The corresponding BET surface areas were 1060, 840 and 698 $m^2\ g^{-1}$, respectively. Similar tendencies were found in the case of the corresponding samples calcined in air at 873 K.

As to the influence of the calcination temperature, it emerges from Table 1 that the calcination procedure at 673 K led to an increased BET surface area and pore volume compared to the raw aerogels. However, calcination at higher temperatures

Table 1 Textural properties and carbon contents of vanadia–silica aero- and xero-gels before and after calcination in flowing air at 673 K and 873 K, respectively

sample	calcination temperature/K	S_{BET} (S_t[a])/ $m^2\ g^{-1}$	$V_{p(N_2)}$ (V_t)[b]/ $cm^3\ g^{-1}$	$\langle d_p \rangle$[c]/ nm	C content[d] (%)
10VLT[e]	—	649 (0)	1.6 (0.0)	10 (15)	6.4
	673	840 (53)	1.8 (0.0)	9 (17)	0.9
	873	728 (37)	1.7 (0.0)	9 (15)	0.2
10VHT	—	839 (0)	3.0 (0.0)	14 (14)	12.3
	673	1060 (0)	3.2 (0.0)	12 (15)	1.3
	873	840 (14)	2.5 (0.0)	12 (16)	0.1
10VLTac	—	789 (0)	1.8 (0.0)	9 (23)	12.4
	673	1032 (195)	1.9 (0.1)	7 (20)	—
	873	879 (150)	1.7 (0.1)	8 (21)	—
10VHTac	—	929 (0)	3.4 (0.0)	15 (23)	11.1
	673	1103 (18)	3.4 (0.0)	12 (25)	—
	873	1037 (0)	3.2 (0.0)	12 (25)	—
10VX	—	535 (89)	0.2 (<0.1)	1 (<2)	8.5
	673	698 (245)	0.2 (0.1)	1 (<2)	1.3
	873	586 (189)	0.1 (0.1)	<1 (<2)	0.1

[a]S_t denotes specific micropore surface area derived from *t*-plot analysis. [b]$V_{p(N_2)}$ designates the BJH cumulative desorption pore volume of pores in the maximum diameter range 1.7–300 nm; V_t denotes specific micropore volume derived from *t*-plot analysis. [c]$\langle d_p \rangle = 4V_{p(N_2)}/S_{BET}$, in addition the graphically assessed pore size maximum of the pore size distribution derived from the desorption branch of the physisorption isotherm are given in parentheses. [d]Carbon contents derived from elemental microanalysis. [e]Quoted for comparison from ref. 1.

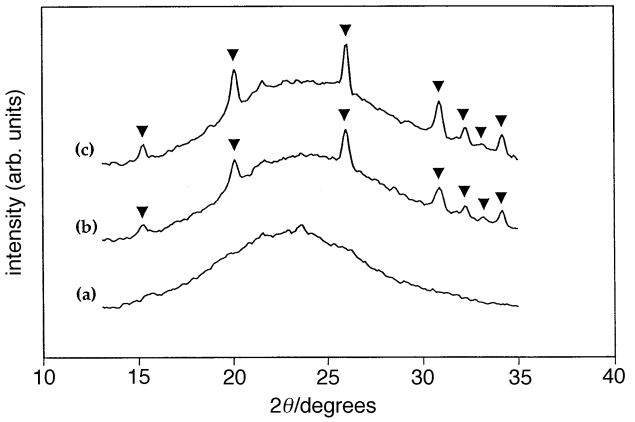

Fig. 2 X-Ray diffraction patterns (Cu-Kα) of the vanadia–silica high-temperature aerogel series 10VHT: (a) as prepared; calcined in air at (b) 673 K and (c) at 873 K (▼, V_2O_5)

caused a significant decline in the BET surface areas and pore volumes of all investigated samples.

X-Ray diffraction

The X-ray diffraction patterns of the high-temperature aerogel series 10VHT, both raw and calcined in air at 673 and 873 K, are depicted in Fig. 2. All raw aerogels and the xerogel sample were X-ray amorphous. Only for 10VHT did calcination at 673 and 873 K lead to well developed V_2O_5 crystallites,[28] which became larger upon increasing the calcination temperature from 673 to 873 K. Sample 10VHTac showed only weak reflections due to crystalline V_2O_5 after calcination at 873 K, whereas for the other samples no indications of V_2O_5 crystallites were visible after calcination.

FTIR spectroscopy

The FTIR spectra and the ratios $R = S_{Si-O-V}/S_{Si-O-Si}$ of the deconvoluted peak areas as estimates for the relative abundance of Si—O—V entities in the mixed oxides (see Experimental) are depicted in Fig. 3. The characteristic values R provide a kind of mixing efficiency which can be related to vanadium dispersion.[1,2]

As to the effect of $V^{III}(acac)_3$ compared to VOTIP used as precursor, the FTIR spectra and estimates of Si—O—V connectivity in Fig. 3 reveal that the $S_{Si-O-V}/S_{Si-O-Si}$ value is markedly smaller for the aerogel sample derived from $V^{III}(acac)_3$ (10VHTac). Note that with the samples derived from $V^{III}(acac)_3$, hydrolysis probably did not take place quantitatively during sol–gel processing, resulting in vanadium species which were extracted during low-temperature supercritical drying. Upon high-temperature supercritical drying these species are likely to be immobilized in the silica matrix owing to the higher temperature (533 K) applied. The effect of the drying method used on the $S_{Si-O-V}/S_{Si-O-Si}$ values of the samples with 10 mass% V_2O_5 and calcined at 873 K show that the higher the drying temperature, the lower the mixing efficiency. The low-temperature aerogel 10VLT and the xerogel showed the highest estimates of vanadia dispersion, whereas the high-temperature aerogel 10VHTac possessed a lower mixing efficiency (Fig. 3).

Raman spectroscopy

The influence of the precursor and of the drying conditions on the structure of the samples is evident from the Raman spectra depicted in Fig. 4 and 5. The spectra of crystalline V_2O_5 and of pure silica are quoted for reference. Besides the bands at 800 cm^{-1} (siloxane bridges)[7,29] and 605 cm^{-1} (three-fold siloxane rings),[7,29] and bands in the range 350–550 cm^{-1}, the pure

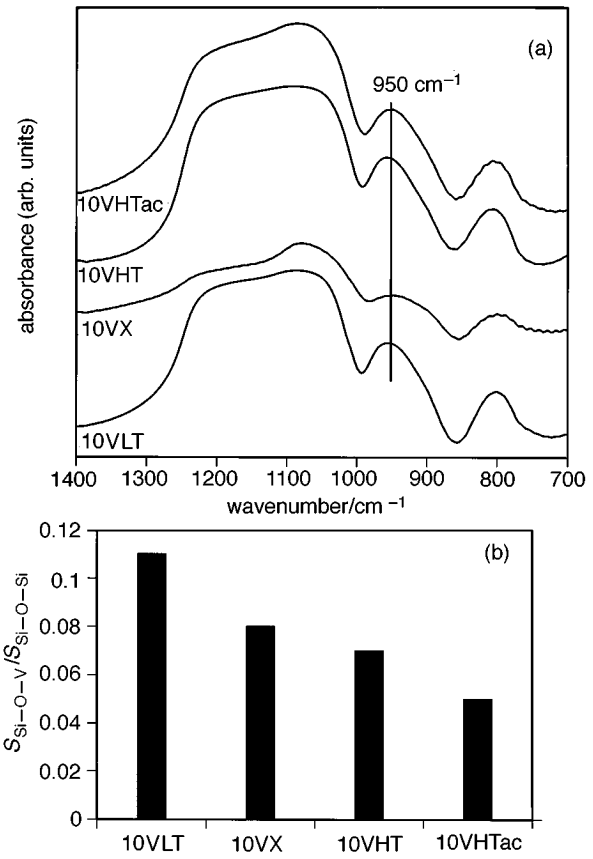

Fig. 3 (a) FTIR analysis of high-temperature (10VHT, 10VHTac) and low-temperature (10VLT) vanadia–silica aerogel samples and of a xerogel sample (10VX), all calcined in air at 873 K. (b) The relative abundance of Si—O—V connectivity is estimated from the ratio $S_{Si-O-V}/S_{Si-O-Si}$ (S_{Si-O-V} and $S_{Si-O-Si}$ represent the peak areas of the Si—O—V band at *ca.* 950 cm^{-1} and the Si—O—Si band at *ca.* 1210 cm^{-1}, respectively).

silica aerogel is characterized by a band at 975 cm^{-1}, assigned to Si—OH vibrations in dehydrated silica.[24,29,30] The Raman spectrum obtained for pure crystalline V_2O_5 vibrations is dominated by strong bands appearing at 995, 700 and 285 cm^{-1} and by less intense bands at 525, 480 and 405 cm^{-1}. A survey of the most prominent spectroscopic features with the corresponding interpretations is listed in Table 2 for the mixed oxide samples.

Both high-temperature aerogels 10VHT and 10VHTac, derived from VOTIP and $V^{III}(acac)_3$, respectively, contained crystalline V_2O_5, as evidenced by the bands at 995, 700, 525, 480, 405 and 285 cm^{-1} (Table 2, Fig. 4). The bands were slightly weaker when $V^{III}(acac)_3$ was used as a precursor. In contrast to 10VHT, however, 10VHTac possessed a distinct band at 1035 cm^{-1} and a weak feature at 920 cm^{-1}. The former has been attributed to ν(V=O) vibrations of pseudo-tetrahedrally coordinated monomeric[31–33] and oligomeric[31] vanadyl species, whereas the latter originates from ν(V=O) of polyvanadate chains and ribbons with tetrahedral or square-pyramidal coordination.[35,36] Both are indicative of well dispersed vanadia species.

The low-temperature aerogels 10VLT and 10VLTac revealed bands typical of silica vibrations (800, 605 cm^{-1}), which were clearly stronger for 10VLTac compared to 10VLT. In addition, both samples showed distinct features at 1030 and 920 cm^{-1}, attributed to well dispersed vanadia species. Compared to VOTIP, the use of $V^{III}(acac)_3$ (lower vanadia loading) led to stronger silica vibrations and weaker vanadia bands (Fig. 4).

The effect of the drying method is illustrated in Fig. 5. Vanadia–silica samples dried at low temperatures, *i.e.* xerogel 10VX and low-temperature aerogel 10VLT, showed Raman

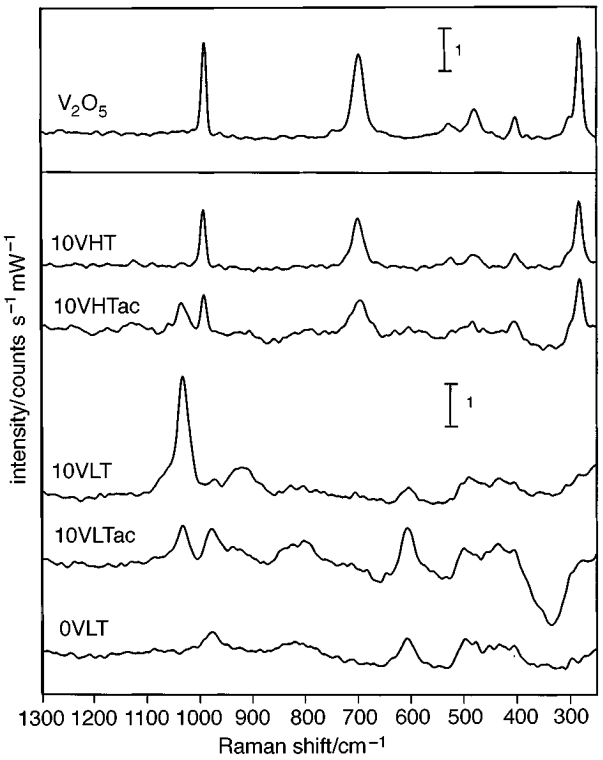

Fig. 4 Raman spectra of a pure silica low-temperature aerogel 0VLT, the vanadia–silica low-temperature aerogels 10VLT and 10VLTac, the vanadia–silica high-temperature aerogels 10VHT and 10VHTac as well as of crystalline V_2O_5 (Fluka; *purum*). All mixed oxides and the pure silica were calcined in air at 873 K. The laser power was 0.1 W for V_2O_5, and 0.9 W for the other samples. Designations of samples are explained in the Experimental section.

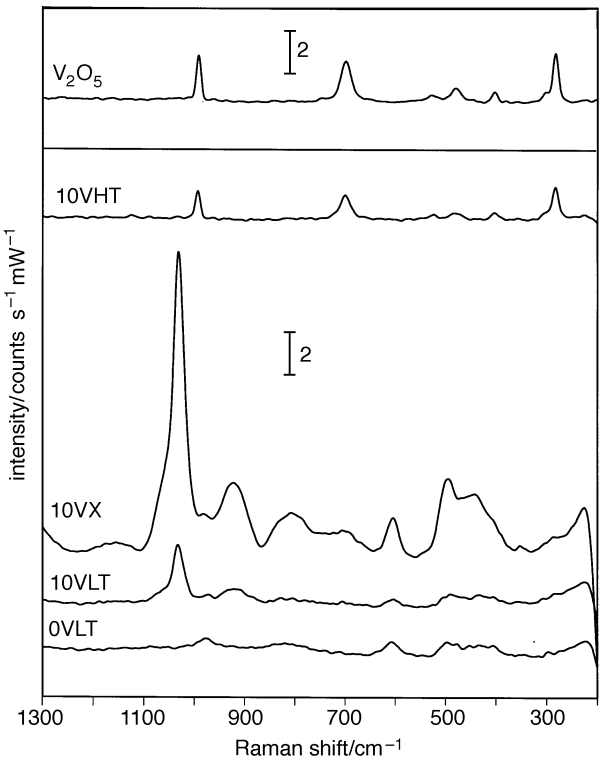

Fig. 5 Raman spectra of differently dried vanadia–silica mixed oxides: high-temperature aerogel 10VHT, xerogel 10VX and low-temperature aerogel 10VLT. Spectra of a pure silica low-temperature aerogel 0VLT and of crystalline V_2O_5 (Fluka; *purum*) are quoted for comparison. All aerogels were calcined in air at 873 K. The laser power was 0.1 W for V_2O_5, and 0.9 W for the other samples. Designations of samples are explained in the Experimental section.

patterns typical of well dispersed vanadia as well as weaker bands due to silica and the band characteristic for Si—OH (975 cm^{-1}). Compared to the evaporatively dried, dense xerogel 10VX, the band intensities of the tenuous aerogel 10VLT were markedly lower. No indication of the presence of crystalline V_2O_5 is seen for these samples. In contrast to the mildly dried mixed oxides, only bands assignable to crystalline V_2O_5 were observed for the high-temperature aerogel (Table 2, Fig. 5).

XPS analysis

XPS analysis was performed to study the influence of the vanadia precursor and of the drying conditions on the nature and the concentration of the surface vanadium species. Measurements were carried out with samples calcined in air at 873 K. For all samples the Si 2p signal of silicon was found at a binding energy of 103.6 eV. XP spectra of the V $2p_{3/2}$ region are shown in Fig. 6 after subtraction of the X-ray-induced satellites of the O 1s peak. The measured peak maxima for the aerogels and the xerogel were located in the binding energy range 517–518.5 eV. The linewidth (FWHM) of the V $2p_{3/2}$ peaks was remarkably larger than the linewidth reported for reference compounds such as V_2O_5 (1.6 eV),[37] indicating a superposition of contributions from different vanadium species. For vanadium in the oxidation state +5, as present in V_2O_5, ranges from 516.8–517.7 eV are reported.[38] Vogt *et al.*[39] measured a binding energy of 517.3 eV for 12.6 mass% V_2O_5–SiO_2. A shift to a lower binding energy of 516.1 eV was observed for a sample containing 7 mass% V_2O_5, which was attributed to an increased concentration of vanadium(IV). A similar low binding energy of 516.6 eV was observed by Huuhtanen *et al.*[40] for a V_2O_5–HfO_2 sample

Table 2 Assignments of the Raman bands for the aero- and xero-gel samples calcined in air at 873 K

10VLT	10VHT	10VLTac	10VHTac	10VX	assignment
1030		1030w	1035w	1030	ν(V=O) of pseudo-tetrahedrally coordinated monomeric[15,31–33] and oligomeric species[31]
	995		995		ν(V=O) in multilayer structures, typical of crystalline V_2O_5[29,33,34]
975		975		975	Si—OH in dehydrated silica[24,29,30]
920		920	920w	920	ν(V=O) of polyvanadate chains and ribbons with tetrahedral or square-pyramidal coordination[35,36]
		800	800	800	siloxane bridges[7,29]
	700		700		crystalline V_2O_5[29,33,34]
605		605		605	three-fold siloxane rings[7,29]
	525		525		crystalline V_2O_5[29,33,34]
	480		480		crystalline V_2O_5[29,33,34]
	405		405		crystalline V_2O_5[29,33,34]
	285		285		crystalline V_2O_5[29,33,34]

w = weak signal.

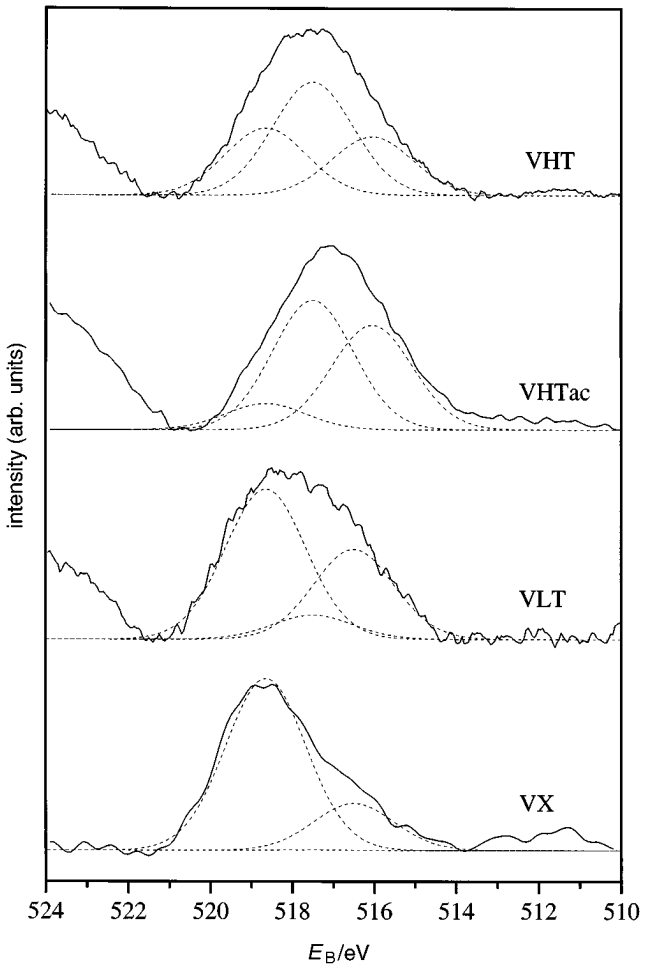

Fig. 6 XPS results of the V $2p_{3/2}$ region of the vanadia–silica mixed oxides 10VLT, 10VHT, 10VHTac and 10VX, all calcined in air at 873 K, after corrections for O 1s satellites. Designations of samples and details of deconvolution are given in the Experimental and Results sections, respectively.

prepared from vanadyl acetylacetonate, indicating a considerable fraction of V^{IV} even after calcination at 723 K. Fierro *et al.*[41] also interpreted a shift to lower binding energies for well dispersed vanadium oxide on silica as being caused by the formation of vanadium(IV) in considerable amounts. Horvath *et al.*[42] investigated several vanadium surface compounds on silica gel [$(SiO)_3V{=}O$ and $(SiO)_3V(O_2)$ structures] by XPS. They reported a shift of the V $2p_{3/2}$ binding energies of up to 2 eV towards higher values in comparison to bulk vanadium compounds in a silica environment to be caused by a strong electron-withdrawing effect of the support on V in surface compounds.

For analysis the XP spectra shown in Fig. 6 were deconvoluted into three peaks with binding energies characteristic of vanadium species interacting strongly with silica (518.6 eV), crystalline V_2O_5 (517.5 eV) and a vanadia species with an oxidation state <5 (516–516.5 eV). The FWHM was held constant at 2.4 eV and a Gaussian profile with 20% contribution of a Lorentz profile was used. The corresponding peaks are included in Fig. 6. Aerogels obtained by high-temperature supercritical drying showed a predominance of bulk type V_2O_5 species. In addition, a substantial amount of partly reduced vanadia species was observed for the sample prepared from the acetylacetonate precursor (10VHTac), whereas significant contributions of both the peaks at 518.6 and 516 eV are found for sample 10VHT prepared from VOTIP. For the samples dried at lower temperatures (10VX, 10VLT), the contribution of vanadium interacting strongly with silica is predominant, besides the lower amounts of partly reduced vanadia species. No indication of crystalline V_2O_5 could be found with the xerogel 10VX. On the basis of a linear correlation between the binding energies of different vanadium oxides with their formal oxidation states presented by Nickl *et al.*,[37] the formal oxidation states of the partly reduced vanadia species represented by the peaks at 516–516.5 eV are estimated to be approximately in the range 4–4.6.

The semiquantitative analysis of the XP spectra showed that all aerogel samples exhibit enrichment of silicon on the surface compared to the bulk concentration. With respect to the surface vanadium content, a decrease from 1.7 atom% V for the high-temperature aerogel 10VHT to 1.2 atom% V for the xerogel (10VX) and the low-temperature aerogel (10VLT) and further to 0.9 atom% V for sample 10VHTac prepared from $V^{III}(acac)_3$ was observed. No indication of surface vanadium was found for sample 10VLTac. The results indicate that the vanadia precursor and the drying procedure markedly influenced the vanadium content on the surface. The highest vanadium surface concentration is obtained when VOTIP is used as a precursor and when high-temperature supercritical drying is applied.

UV–VIS diffuse reflectance spectroscopy

Kubelka–Munk-transformed diffuse reflectance spectra of mixed oxide samples dried by different methods and calcined at 873 K are represented in Fig. 7. In general, the UV–VIS spectra of vanadium ions are characterized by charge-transfer (CT) transitions between the central vanadium atoms and oxygen ligands.[43,44] The energy of these transitions is influenced strongly by the number and nature of ligands surrounding the central vanadium ion, and thus provides information on the local structure of vanadium.[45] Isolated species generally give rise to CT transitions in a higher energy range (higher frequencies) than polymeric species.[43] Transitions falling in the range 30 000–35 000 cm^{-1} are associated with species with pseudo-tetrahedral coordination, whereas for octahedrally coordinated V^V species the CT transition is expected at lower frequencies.[43,46] The CT transition for V^{IV} occurs in the range 35 000–40 000 cm^{-1}[46] and overlaps with the absorption of silica. The d–d transition of VO^{2+} ions arise at *ca.* 13 000 and near 16 000 cm^{-1}. The intensities of the latter are generally about 10 times lower than those of CT transitions.[46]

UV–VIS analysis of the samples showed a broad absorption at *ca.* 34 000 cm^{-1} with a shoulder at *ca.* 30 000 cm^{-1}, characteristic of pseudo-tetrahedrally coordinated VO^{3+} species.[31,43,46] As discussed above, the observed shift of the spectra to lower frequencies indicates an increase of polymeric

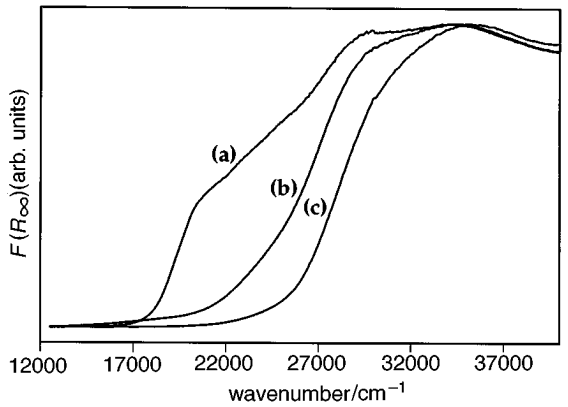

Fig. 7 Diffuse-reflectance UV–VIS spectra of samples calcined in air at 873 K: (a) high-temperature aerogel 10VHT, (b) low-temperature aerogel 10VLT and (c) xerogel 10VX. The samples were pretreated at 125 mbar and 410 K for 1 h before measurements. Designations of samples are explained in the Experimental section.

type species in the order 10VHT > 10VLT > 10VX. A shoulder at 20 500 cm^{-1} for the high-temperature aerogel 10VHT indicates the presence of crystalline V_2O_5,[31,43,47] which is in accordance with the XRD and the vibrational spectroscopy results. No clear indication for the presence of V^{IV} is seen in the spectra owing to the reasons mentioned above.

Discussion

Influence of the vanadia precursor

Vanadium(V) oxide triisopropoxide (VOTIP) and vanadium(III) acetylacetonate [$V^{III}(acac)_3$] were used as precursors possessing different formal charges, coordination numbers, steric and inductive effects of the ligands, and partial charges, all of which influence hydrolysis and (poly-)condensation.[7,8,13,48]

The use of $V^{III}(acac)_3$ as a precursor, where all alkoxy groups are substituted by acetylacetone as a chelating ligand, distinctly decelerates hydrolysis compared to VOTIP. The observed low vanadia loading of 1.5 mass% for sample 10VLTac indicates that with these samples hydrolysis presumably did not take place quantitatively during the sol–gel process, resulting in vanadium species which were extracted during low-temperature supercritical drying, whereas upon high-temperature supercritical drying these species are likely to be immobilized in the silica matrix owing to the high-temperature conditions (533 K) and the presence of residual water. Moreover, oxidation of $V^{III}(acac)_3$ to vanadyl acetonate (V^{IV}) is expected to take place during the preparation.

The use of $V^{III}(acac)_3$ instead of VOTIP as the vanadia precursor resulted in slightly higher pore volumes, BET surface areas and pore size maxima for both high-temperature and low-temperature aerogels (Table 1). The latter shows properties typical of vanadia silica aerogels with low vanadia loadings.[1] As for the structural properties, the ratio $R = (S_{Si-O-V}/S_{Si-O-Si})$ and the vanadium surface concentrations of 10VHTac were lower than those of the corresponding samples prepared with VOTIP (Fig. 3). The high-temperature aerogel 10VHT derived from VOTIP, however, contained well developed V_2O_5 crystallites after calcination in air at 673 K, whereas 10VHTac remained X-ray amorphous. Thus, it seems that the acetylacetone ligands stabilised the vanadium constituent in a dispersed manner.

Influence of the drying method

The lower surface areas and pore volumes of the vanadia–silica xerogel series combined with low $\langle d_p \rangle$ values is explained by the occurrence of differential capillary forces in the gel network during the evaporative drying (Table 1, Fig. 1).[11] The prominent meso- to macro-porosity of the high-temperature aerogels is likely to originate from the increased water reactivity under the conditions of high-temperature supercritical drying (533 K). On the molecular scale, water in particular can cause dissolution, reprecipitation, depolymerisation, repolymerisation, alkoxylation and enhanced syneresis (network densification), leading to chemical and/or restructuring phenomena in these materials.[13] Such processes include Ostwald ripening, coalescence–coarsening, sintering and syneresis resulting in larger pore volumes. The low-temperature aerogels, obtained by semicontinuously extracting the entrapped alcohol with supercritical CO_2 at 313 K, were mesoporous with low microporosity compared to the evaporatively dried xerogels. The BET surface areas and nitrogen pore volumes of the low-temperature aerogel series were lower than those of the corresponding high-temperature samples. It is supposed that stresses within the gel network due to adsorption of the extraction medium during depressurisation are the most probable reason for these effects.[49]

The influence of the drying method on the estimated Si—O—V connectivity may be inferred from the structural properties of V_2O_5 and SiO_2. The average bond lengths are *ca.* 1.6 Å for both V—O and Si—O, the ionic radii are 0.74, 0.59 and 0.42 Å for V^{3+}, V^{5+} and Si^{4+},[50] respectively. Consequently, substitution of Si for V in the silica matrix seems to be possible. However, the experimentally determined crystallisation temperature (T_{ch}) compared with the adiabatic nucleation temperature (T_n) is used to classify the glass forming properties of oxides.[51,52] Accordingly, SiO_2 represents a good glass former ($T_{ch} > T_n$), whereas V_2O_5 has comparatively poor glass-forming properties ($T_{ch} < T_n$). This restriction of amorphicity (glass-forming properties) for V_2O_5 is likely to be a decisive factor, limiting the complete miscibility of vanadium ions in the silica matrix.

The sol–gel products of the high-temperature aerogels were exposed to 533 K during supercritical drying. For the high-temperature aerogels 10VHT and 10VHTac this high temperature was apparently sufficient to transform the metastable structure of the sol–gel system into a thermodynamically equilibrated state *via* segregation–agglomeration resulting in crystalline V_2O_5 after calcination in air at 873 K (Fig. 2 and 4). The processes concerned have already been mentioned. In contrast, the highly dispersed state of the sol–gel system could be preserved in both the low-temperature aerogels processed at 313 K and the xerogels dried at 373 K, because thermodynamic equilibration was kinetically hindered by the low temperatures applied.[13] Similar tendencies were found for titania–silica mixed oxides.[2] However, there is a larger difference in the ratios $S_{Si-O-Ti}/S_{Si-O-Si}$ of the differently dried samples, than in the corresponding ratios $S_{Si-O-V}/S_{Si-O-Si}$. A probable explanation is that the characteristics of silica and titania differ more than those of silica and vanadia. The electronegativities of V, Ti and Si are 1.6, 1.3 and 1.8, respectively,[8] and the ionic radius of Ti^{4+} (0.68 Å[50]) is larger than that of V^{5+} (0.59 Å[50]).[53] These findings are confirmed by XRD. The uncalcined vanadia–silica high-temperature aerogel 10VHT was X-ray amorphous (Fig. 2), whereas the corresponding uncalcined titania–silica high-temperature aerogel 10HT contained well developed anatase crystallites.[2]

Effect of calcination temperature

It emerges from our previous study, which included thermal analysis,[1] and from Table 1 that the increase in BET surface area after calcination in air at 673 K is due to the removal of organic residues, rendering the surface accessible for the physisorption of nitrogen.[54] The subsequent decrease in BET surface area and pore volume at temperatures > 673 K was likely to result from processes such as Ostwald ripening, coalescence–coarsening, sintering and syneresis.[1]

With regard to the thermal stability of the vanadia dispersion, X-ray diffraction and Raman spectroscopy showed that calcination in air up to 873 K did not lead to crystallisation of vanadia to V_2O_5, except for the high-temperature aerogels (Fig. 2 and 4). Raman (Fig. 5), XP (Fig. 6) and UV–VIS diffuse reflectance spectra (Fig. 7) were recorded with samples calcined in air at 873 K. The measurements revealed that the three-dimensionally distributed vanadia constituent of the low-temperature aerogel 10VLT and the xerogel 10VX remain well dispersed even after calcination at elevated temperatures. Therefore the synthesis of highly mixed oxides *via* the sol–gel method offers a potent means for controlling segregation, agglomeration and crystallisation of well dispersed vanadia during calcination at relatively high temperatures. This behaviour is an advantage compared to two-dimensional systems prepared by, for example, impregnation where weak interactions of vanadia with the silica surface easily tends to form agglomerates.[55]

Conclusions

It has been shown that the choice of the precursor significantly influences the properties of the resulting sol–gel product. The use of vanadium(III) acetylacetonate as precursor, with much lower reactivity compared to vanadium(V) oxide triisopropoxide, resulted in vanadia–silica aerogels with textural properties similar to silica, and lower surface concentrations of vanadium compared to corresponding samples prepared with vanadium(V) oxide triisopropoxide.

The drying method employed influences both the textural properties and the vanadia dispersion. The conditions during high-temperature supercritical drying led to increased water reactivity and thus to prominent meso- to macro-porosity of the resultant aerogels. Concerning the dispersion, the temperature applied for high-temperature supercritical drying (533 K) is apparently sufficient to transform the metastable structure of the sol–gel product into a thermodynamically more equilibrated state *via* segregation–agglomeration leading to crystalline V_2O_5 after calcination in air at 873 K, as shown by X-ray diffraction and Raman spectroscopy. The low-temperature aerogels derived from extraction with supercritical CO_2 at 313 K were mesoporous with low microporosity compared to the evaporatively dried xerogels. The shrinkage of these aerogels is probably caused by adsorption of the extraction medium during depressurisation. In contrast to the high-temperature aerogels, the kinetic hindrance of thermodynamic equilibration during calcination in air up to 873 K preserves the highly dispersed state of the sol–gel system for both the low-temperature aerogels extracted at 313 K and the xerogel dried at 373 K. The marked effects of vanadia precursor, drying method and calcination temperature on the structural and morphological properties of vanadia–silica revealed that the preparation of highly mixed oxides offers a potent means for controlling segregation, agglomeration and/or crystallisation of the three-dimensionally distributed vanadia constituent.

The authors thank Carsten Stöcker for preparing the high-temperature aerogels and Ulrich Göbel for the XPS measurements. Financial support by the Swiss National Science Foundation (2129-041850.94) is kindly acknowledged.

References

1 D. C. M. Dutoit, M. Schneider, P. Fabrizioli and A. Baiker, *Chem. Mater*., 1996, **8**, 734.
2 D. C. M. Dutoit, M. Schneider and A. Baiker, *J. Catal*., 1995, **153**, 165.
3 M. Aizawa, Y. Nosaka and N. Fujii, *J. Non-Cryst. Solids*, 1991, **128**, 77.
4 J. B. Miller, S. T. Johnston and E. I. Ko, *J. Catal*., 1994, **150**, 311.
5 D. C. Bradley, R. C. Mehrotra and D. P. Gaur, *Metal Alkoxides*, Academic Press, London, 1978.
6 C. Sanchez and J. Livage, *New J. Chem*., 1990, **14**, 513.
7 C. J. Brinker and G. W. Scherer, *Sol–Gel Science—The Physics and Chemistry of Sol–Gel Processing*, Academic Press, San Diego, 1990.
8 J. Livage, M. Henry and C. Sanchez, *Prog. Solid State Chem*., 1988, **18**, 259.
9 D. A. Ward and E. I. Ko, *Ind. Eng. Chem. Res*., 1995, **34**, 421.
10 R. Hutter, T. Mallat and A. Baiker, *J. Catal*., 1995, **153**, 177.
11 G. W. Scherer, *J. Am. Ceram. Soc*., 1990, **73**, 3.
12 B. Rangarajan and C. T. Lira, *J. Supercrit. Fluids*, 1991, **4**, 1.
13 M. Schneider and A. Baiker, *Catal. Rev. Sci. Eng*., 1995, **37**, 515.
14 *TRC Thermodynamic Tables—Non-Hydrocarbons*, Thermodynamics Research Centre, Texas A&M University System, College Station, Texas, 1992, vol. IV, p. i–5000.
15 K. Tran, M. A. Hanning-Lee, A. Biswas, A. E. Stiegman and G. W. Scott, *J. Am. Chem. Soc*., 1995, **117**, 2618.
16 A. Zecchina, G. Spoto, S. Bordiga, A. Ferrero, G. Pertini, G. Leofanti and M. Padovan, in *Zeolite Chemistry and Catalysis*, ed. P. A. Jacobs, Elsevier, Amsterdam, 1991, p. 251.
17 E. Astorino, J. B. Peri, R. J. Willey and G. Busca, *J. Catal*., 1995, **157**, 482.
18 G. Bellussi and M. S. Rigutto, in *Advanced Zeolite Science and Applications, Stud. Surf. Sci. Catal*., 1994, **85**, 177.
19 P. R. Hari Prasad Rao, R. Kumar, A. V. Ramaswamy and P. Ratnasamy, *Zeolites*, 1993, **13**, 663.
20 P. R. Hari Prasad Rao, A. V. Ramaswamy and P. Ratnasamy, *J. Catal*., 1992, **137**, 225.
21 A. Tuel and Y. Ben Taarit, *Appl. Catal. A, General*, 1993, **102**, 201.
22 R. Neumann, M. Chava and M. Levin, *J. Chem. Soc., Chem. Commun*., 1993, 1685.
23 A. E. Stiegman, H. Eckert, G. Plett, S. Sam Kim, M. Anderson and A. Yavrouian, *Chem. Mater*., 1993, **5**, 1591.
24 D. Scarano, A. Zecchina, S. Bordiga, F. Geobaldo, G. Spoto, G. Pertini, G. Leofanti, M. Padovan and G. Tozzola, *J. Chem. Soc., Faraday Trans*., 1993, **89**, 4123.
25 A. Duran, C. Serna, V. Fornes and J. M. Fernandez-Navarro, *J. Non-Cryst. Solids*, 1986, **82**, 69.
26 M. Schraml-Marth, K. L. Walther, A. Wokaun, B. E. Handy and A. Baiker, *J. Non-Cryst. Solids*, 1992, **143**, 93.
27 K. S. W. Sing, D. H. Everett, R. A. W. Haul, L. Moscou, R. A. Pierotti, J. Rouquérol and T. Siemieniewska, *Pure Appl. Chem*., 1985, **57**, 603.
28 ICDD Mineral Powder Diffraction Data File 9-0387, Newtown Square, Pennsylvania.
29 N. Das, H. Eckert, H. Hu, I. E. Wachs, J. F. Walzer and F. J. Feher, *J. Phys. Chem*., 1993, **97**, 8240.
30 D. L. Wood and E. M. Rabinovich, *Appl. Spectrosc. C*, 1989, **43**, 263.
31 M. Schraml-Marth, A. Wokaun, M. Pohl and H-L. Krauss, *J. Chem. Soc., Faraday Trans*., 1991, **87**, 2635.
32 I. E. Wachs, G. Deo, M. A. Vuurman, H. Hu, D. Soung Kim and J-M. Jehng, *J. Mol. Catal*., 1993, **82**, 443.
33 G. T. Went, S. T. Oyama and A. T. Bell, *J. Phys. Chem*., 1990, **94**, 4240.
34 C. Sanchez, J. Livage and G. Lucazeau, *J. Raman Spectrosc*., 1982, **12**, 68.
35 J-M. Jehng and I. E. Wachs, *Catal. Lett*., 1992, **13**, 9.
36 U. Scharf, M. Schraml-Marth, A. Wokaun and A. Baiker, *J. Chem. Soc., Faraday Trans*., 1991, **87**, 3299.
37 J. Nickl, R. Schlögl, A. Baiker, H. Knözinger and G. Ertl, *Catal. Lett*., 1989, **3**, 379.
38 C. D. Wagner, W. M. Riggs, L. E. Davis, J. F. Moulder and G. E. Muilenberg, *Handbook of X-Ray Photoelectron Spectroscopy*, Perkin-Elmer Corporation, Eden Prairie, MN, 1979.
39 E. T. C. Vogt, M. DeBoer, A. J. Van Dillen and J. W. Geus, *Appl. Catal*., 1988, **40**, 255.
40 J. Huuhtanen, M. Sanati, A. Andersson and S. L. T. Andersson, *Appl. Catal*., 1993, **97**, 197.
41 J. L. G. Fierro, L. A. Gambaro, T. A. Cooper and G. Kremenic, *Appl. Catal*., 1983, **6**, 363.
42 B. Horvath, J. Struntz, J. Geyer and E. G. Horvath, *Z. Anorg. Allg. Chem*., 1981, **483**, 181.
43 M. Morey, A. Davidson, H. Eckert and G. Stucky, *Chem. Mater*., 1996, **8**, 486.
44 M. Iwamoto, H. Furukawa, K. Matsukami, T. Takenata and S. Kagawa, *J. Am. Chem. Soc*., 1983, **105**, 3719.
45 G. Rasch, H. Bögel and C. Rein, *Z. Phys. Chem. (Leipzig)*, 1987, **259**, 955.
46 G. Busca, G. Centi, L. Marchetti and F. Trifiro, *Langmuir*, 1986, **2**, 568.
47 B. Jonson, B. Rebenstorf, R. Larsson and S. L. T. Andersson, *J. Chem. Soc., Faraday Trans*., 1988, **84**, 1897.
48 H. Hirashima, K. Tsukimi and R. Muratake, *J. Ceram Soc. Jpn. Int. Ed*., 1989, **97**, 232.
49 B. Rangarajan and C. T. Lira, *Mater. Res. Soc. Symp. Proc*., 1992, **271**, 559.
50 *CRC Handbook of Chemistry and Physics*, ed. R. C. Weast, M. J. Astle and W. H. Beyer, CRC Press, Boca Raton, FL, 1987.
51 E. Meyer, E. D. Zanotto and M. A. Aegerter, *J. Non-Cryst. Solids*, 1990, **121**, 279.
52 E. D. Zanotto, *J. Non-Cryst. Solids*, 1992, **147&148**, 820.
53 G. Centi, S. Perathoner, F. Trifiro, A. Aboukais, C. F. Aissi and M. Guelton, *J. Phys. Chem*., 1992, **96**, 2617.
54 M. Yamane, S. Aso, S. Okano and T. Sakaino, *J. Mater. Sci*., 1979, **14**, 607.
55 A. Baiker, P. Dollenmeier, M. Glinski, A. Reller and V. K. Sharma, *J. Catal*., 1988, **111**, 273.

Paper 6/06226A; *Received* 10*th September*, 1996